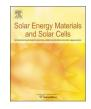


Contents lists available at ScienceDirect

Solar Energy Materials and Solar Cells

journal homepage: www.elsevier.com/locate/solmat



Defective BiFeO₃ with surface oxygen vacancies: Facile synthesis and mechanism insight into photocatalytic performance



Da Chen, Feng Niu, Laishun Qin*, Sen Wang, Ning Zhang, Yuexiang Huang*

College of Materials Science and Engineering, China Jiliang University, Hangzhou 310018, Zhejiang, PR China

ARTICLE INFO

Surface oxygen vacancy

Photocatalytic degradation

Photocatalytic mechanism

BiFeO3 nanocrystals

Hydrogenation

Keywords:

ABSTRACT

Oxygen vacancies particularly for those located on the photocatalyst surface are believed to play an important role in its photocatalytic process. In this work, surface oxygen vacancies were introduced into hydrothermallysynthesized BiFeO₃ (BFO) nanocrystals through high pressure hydrogenation treatment, and with increasing hydrogenation temperature the oxygen vacancy concentration would increase. The X-ray diffraction (XRD) results indicated no pronounced structure change when the hydrogenation temperature was below 200 °C. The formation of surface oxygen vacancies on BFO nanocrystals was verified by a variety of techniques such as highresolution transmission electron microscopy (HRTEM), X-ray photoelectron spectroscopy (XPS), electron paramagnetic resonance (EPR) and Kelvin probe force microscopy (KPFM). The hydrogenated BFO nanocrystals exhibited nearly four times methyl orange (MO) photodegradation efficiency higher than pristine BFO under visible light irradiation, and the inherent correlation between surface oxygen vacancies and enhanced photocatalytic activity was established. Our findings demonstrate that the formation of surface oxygen vacancies on the hydrogenated BFO nanocrystals could narrow the band gap of BFO resulting in the improved light absorption capability, act as trapping centers for photoinduced electrons thus to facilitate the separation of the photogenerated electron-hole pairs as well as the production of predominant active species (hydroxyl radicals) for MO photodegradation, suppress the recombination of photogenerated electrons and holes, and also favor the adsorption of MO molecules. All these factors could contribute to the observed enhanced photocatalytic activity of the hydrogenated BFO nanocrystals for MO degradation. In addition, the as-formed surface oxygen vacancies were also stable at room temperature.

1. Introduction

The interest of developing semiconductor metal oxides as photocatalysts for environmental purification and solar energy conversion arises from their good chemical stability, simplicity of synthesis, and relatively low cost [1]. For example metal oxide photocatalysts including TiO₂ [2], ZnO [3], WO₃ [4], BiVO₄ [5], Fe₂O₃ [6] have been explored for applications in removal or degradation of environmental pollutants, splitting water to generate hydrogen energy and reducing carbon dioxide to fuel molecules. Bismuth ferrite (BiFeO3, noted as BFO), which is well-recognized as a multiferroic material used in multiferroic memories [7], has been considered as a potential photocatalyst largely due to its narrow band gap ($\sim 2.5 \text{ eV}$) [8]. In contrast to the wide band gap (~ 3.2 eV) of the most-investigated TiO₂ photocatalyst which can only respond to ultraviolet irradiation, the narrow band gap of BFO allows its visible light response to be possible which apparently will increase solar light harvesting efficiency. In fact, the visible light photocatalytic activities of BFO for organic pollutants degradation have been already demonstrated in recent reports [9–11]. However, the photocatalytic efficiency of BFO is still low. This is largely attributed to the poor carrier mobility in BFO material which limits the separation and transport efficiency of photo-induced electron/hole carriers. Therefore, further improving the photocatalytic activity of BFO materials is still a big challenge.

It is widely recognized that oxygen vacancies especially for those located in particle surfaces would play an important role in photocatalytic process [12]. Mao and co-workers [13] used a high pressure hydrogenation process to yield a disorder layer on TiO_2 nanoparticle surface where substantial oxygen vacancies were formed. The obtained black TiO_2 demonstrated considerable solar-driven hydrogen evolution capability from water splitting. Wang et al. [14] used a simple heat treatment process to prepare oxygen vacancy-rich ZnO nanocrystals. The presence of oxygen vacancies in ZnO led to a narrow band gap and thus facilitate its visible light absorption. Lv and co-workers [15] reported that the introduction of oxygen vacancies in BiPO₄ nanorods by a vacuum deoxidation process could broaden the valence band, thus

http://dx.doi.org/10.1016/j.solmat.2017.06.021

^{*} Corresponding authors. E-mail addresses: qinlaishun@cjlu.edu.cn (L. Qin), yuexiang65@hotmail.com (Y. Huang).

Received 20 January 2017; Received in revised form 15 June 2017; Accepted 16 June 2017 0927-0248/ @ 2017 Elsevier B.V. All rights reserved.

leading to an enhanced photocatalytic performance. Recently Tan et al. [16] also introduced oxygen vacancies into pervoskite $SrTiO_3$ nanocrystals using NaBH₄ as a reducing agent, and further confirmed the favorable effect of oxygen vacancies on the photocatalytic activity. Though the favorable effect of oxygen vacancies on photocatalytic activity have been observed in various metal oxides, it is important to note that the understanding of such a favorable effect is still very poor, especially for the relationship between oxygen vacancies and photocatalytic activities.

Herein, surface oxygen vacancies were introduced into hydrothermally-synthesized BFO nanocrytals by a high pressure hydrogenation process. The presence and enhanced density of surface oxygen vacancies by hydrogenation were then verified via various characterization techniques. The inherent correlation between surface oxygen vacancies and photocatalytic activities of the hydrogenated BFO nanocrystals for the first time was established.

2. Experimental

2.1. Hydrothermal synthesis of BiFeO₃ nanoparticles

All chemicals were of analytical grade without any further purification. BFO nanoparticles were synthesized through a hydrothermal process. Typically, bismuth nitrate (Bi(NO₃)₃·5H₂O) and ferric nitrate (Fe(NO₃)₃·9H₂O) with a stoichiometric ratio were dissolved in distilled water. The NaOH aqueous solution (7.5 M) was dropwisely added into the mixed solution at a rate of 1 mLmin^{-1} through a burette to get a yellowish-brown-colored precipitate. After being washed with distilled water and ethyl alcohol several times, dried in an oven at 70 °C for 5 h and ground by a pestle and mortar, the precipitate was dispersed in polyvinyl pyrrolidone (PVP) aqueous solution under stirring, and the stirring was kept for 10 h to obtain a suspension. 3 M NaOH solution as a mineralizer was then added to the above suspension, and finally the mixed suspension was transferred into a hydrothermal reactor. The reactor was then sealed and maintained at 200 °C for 3 h. After being cooled down to room temperature, the process of filtration, washing with distilled water and drying in an oven at 80 °C for 12 h was operated to obtain BFO nanoparticles.

2.2. Hydrogenation of BiFeO₃ nanoparticles

Hydrogenation of BFO nanoparticles was performed in a hydrogenation furnace. 1 g of as-prepared BiFeO₃ powder was put in a stainless steel reactor which was then connected to the vacuum system. After being evacuated by a vacuum pump to 10 Pa, the reactor was heated to a given temperature at a heating rate of 5 °C min⁻¹ and then was filled with hydrogen (purity higher than 99.99%) at a pressure of 2.0 MPa. After being kept for 8 h, the high pressure hydrogen was relieved and the BFO sample was taken out from the reactor after the reactor was cooled down to room temperature. The as-hydrogenated BFO samples were denoted as HB-*T*-*P*-*t*, where *T*, *P* and *t* were the reaction temperature (*T* = 120, 150, 180, 200 °C), pressure (*P* = 2.0 MPa) and hydrogenation time (*t* = 8 h), respectively.

2.3. Characterizations

X-ray powder diffraction (XRD) was performed on a Bruker D2 Xray diffractometer using Cu K α radiation. The UV–visible diffuse reflectance spectra (UV–vis DRS) of the samples were recorded on a UV–visible spectrophotometer (Shimadzu UV-3600) equipped with an integrating sphere. High resolution transmission electron microscopy (TEM) was operated on a field emission transmission electron microscope (JEOL, JEM-2100) at an accelerating voltage of 200 kV. The chemical states present in BFO and the hydrogenated samples were analyzed using a PHI 5000 Versa Probe X-ray photoelectron spectrometer with Al K α radiation, and C 1s (284.6 eV) was used to calibrate

the peak position. In situ electron paramagnetic resonance (EPR) was recorded at ambient temperature on a Bruker EPR A300 spectrometer. Kelvin probe force microscopy (KPFM) experiments were performed at room temperature and under ambient conditions using an Atomic Force Microscope (Veeco Multimode V). A conductive Co/Cr-coated tip with a resonant frequency of 75 kHz and a spring constant of 2.8 N/m (MESP cantilever, Bruker) was used for KPFM measurement in noncontact mode operation. For KPFM experiments, the sample powder was carefully dispersed on the surface of precleaned ITO conductive glass. Thermogravimetric analysis (TGA) was carried out in a temperature range of 25–800 °C under flowing O₂ with a heating rate of 10 °C min⁻¹ on a Mettler Toledo SMP/PF7458/MET/600W instrument. Room temperature photoluminescence (PL) spectra were recorded on a Hitachi High-Tech F-7000 fluorescence spectrophotometer with a xenon lamp as an excitation source (Excitation wavelength λ = 404 nm).

2.4. Photoelectrochemical evaluation

The photocatalytic activities of pristine BFO and hydrogenated BFO samples were evaluated by monitoring the photocatalytic degradation of methyl orange (MO) in aqueous solutions under visible light irradiation under a neutral pH condition. A 300 W Xe lamp equipped with an optical filter ($\lambda \ge 420$ nm) was employed as the visible light source. An amount of 0.3 g of the catalyst was added into 100 mL of 5 mg L^{-1} MO solution in a quartz glass reactor, which was cooled by refluxing water to prevent any thermal catalytic effect. The photoreaction vessel was then exposed to visible light irradiation under ambient conditions with an average intensity of 15 mW cm^{-2} produced by a 300-W Xenon lamp equipped with an optical filter ($\lambda \ge 420$ nm), which was positioned 25 cm away from the vessel. The irradiance intensity was measured by a radiometer (FZ-A, Photoelectric Instrument Factory of Beijing Normal University, China). Before the light irradiation, the suspension was ultrasonically dispersed in dark for 30 min and then magnetically stirred for 30 min to achieve the adsorption-desorption equilibrium. At given time intervals, 4 mL of suspension was collected and centrifuged at 10,000 rpm for 30 min to remove the catalyst powders. To estimate the degradation efficiency, the absorbancy of the supernatant was detected by measuring the maximum absorbance at 464 nm using a spectrophotometer (model: 722, Precision Instruments Co., Ltd. Shanghai, China).

For photocurrent measurements, the working photoelectrodes were fabricated by doctor blading a slurry, which was prepared by mixing the obtained photocatalyst powder and a polymer binder (PVDF) at a weight ratio of 90:10 using *N*-methyl-2-pyrrolidinone (NMP) as a solvent, on F-doped SnO₂ (FTO) conductive glass with an active area of 1.0 \times 2.0 cm², followed by drying in vacuum at 60 °C for 24 h. Photocurrent measurements were recorded on a CHI660E electrochemical station at 0.0 V potential bias (vs. SCE) using the standard three electrode system with the working photoelectrode, a saturated calomel electrode (SCE) as the reference electrode, and a platinum wire as counter electrode in 0.5 M Na₂SO₄ aqueous solution under visible light ($\lambda \geq$ 420 nm) irradiation.

3. Results and discussion

3.1. Structure evolution

Fig. 1 shows the XRD patterns of the BFO nanoparticles before and after high pressure hydrogenation under different temperatures. It can be seen that all diffraction peaks of the pristine BFO nanoparticles could be indexed by a rhombohedral phase with the space group *R3c* (JCPDS no. 86-1518), indicating that single crystalline BFO phase was obtained by the present hydrothermal process. Such a BFO crystal structure would be maintained when the hydrogenation temperature was below 200 °C. When the hydrogenation temperature was increased to 200 °C,

Download English Version:

https://daneshyari.com/en/article/4758692

Download Persian Version:

https://daneshyari.com/article/4758692

Daneshyari.com